



Cenozoic deep crust in the Pamir

Jennifer Schmidt^a, Bradley R. Hacker^{a,*}, Lothar Ratschbacher^b, Konstanze Stübner^b, Michael Stearns^c, Andrew Kylander-Clark^c, John M. Cottle^c, A. Alexander G. Webb^d, George Gehrels^e, Vladislav Minaev^f

^a Earth Science, University of California, Santa Barbara, 93106, USA

^b Geologie, TU Bergakademie Freiberg, D-09599 Freiberg, Germany

^c Earth Science, University of California, Santa Barbara, CA, USA

^d Geology and Geophysics, Louisiana State University, Baton Rouge, LA 70803, USA

^e Department of Geosciences, University of Arizona, Tucson, AZ 85721, USA

^f Geology, Tajik Academy of Science, Dushanbe, Tajikistan

ARTICLE INFO

Article history:

Received 31 August 2011

Received in revised form 20 October 2011

Accepted 21 October 2011

Available online 22 November 2011

Editor: T.M. Harrison

Keywords:

Pamir
metamorphic petrology
geochronology
exhumation
crustal recycling

ABSTRACT

Multiple high-grade crystalline domes across the Pamir contain Barrovian facies-series metapelites with peak metamorphic assemblages of garnet + kyanite ± staurolite + biotite + oligoclase ± K-white mica. Thermobarometry yields pressures of 6.5–8.2 kbar and temperatures of 600–650 °C for the Kurgovat dome in the northwestern Pamir, 9.4 kbar and 588 °C for the west-central Yazgulom dome, 9.1–11.7 kbar and 700–800 °C for the east-central Muskol dome, and 6.5–14.6 kbar and 700–800 °C for the giant Shakhhdara dome in the southwestern Pamir. These new data indicate exhumation of the Pamir crystalline domes from crustal depths of ~30–40 km. New titanite, monazite and zircon geochronology, in conjunction with published ages, illustrate that this metamorphism is Oligocene–Miocene in all but the Kurgovat dome (where it is Triassic). If the Pamir had a pre-collisional crustal thickness less than 30 km and if the India–Asia convergence within the Pamir is less than 600 km, the current 70 km-thick crust could have been created by plane strain with no net gain or loss of material. Alternatively, if the pre-collisional crustal thickness was greater than 30 km or India–Asia convergence within the Pamir is more than 600 km, significant loss of continental crust must have occurred by subhorizontal extrusion, erosion, or recycling into the mantle. Crustal recycling is the most likely, based on deep seismicity and Miocene deep crustal xenoliths.

© 2011 Elsevier B.V. All rights reserved.

1. Introduction

Much of our understanding of active continent–collision zones has been derived from study of the Tibet Plateau, especially its southern margin, the Himalaya. Tibet, however, has undergone minimal Cenozoic erosion, such that the processes active in the deep levels of the collision zone remain largely a matter of conjecture. In contrast, the Pamir, farther west in the same collision zone (Fig. 1), are deeply dissected and expose large domains of high-grade crystalline rock. The Pamir are virtually unknown compared to Tibet, but the large exposures of crystalline rock likely have much to tell us about processes in the deep crust of continent collision zones.

Tibet and the Pamir both have 70 km-thick crust (Mechie et al., 2011, in review; Schurr et al., 2009) and both absorbed ~2100–1800 km of Cenozoic India–Asia convergence (Johnson, 2002; Le Pichon et al., 1992). The amounts of internal shortening are radically different however. Cenozoic shortening within Tibet is ~300–500 km

(DeCelles et al., 2002), or ~19–28% shortening for the 1300 km N–S ‘width’ of Tibet (Fig. 2A). Cenozoic convergence within the Pamir is difficult to quantify because of the dearth of investigations; however, if the postulated ~300 km southward underthrusting of the Tajik Depression (Burtman and Molnar, 1993), ~700 km northward subduction of Indian lithosphere (Negredo et al., 2007), and <200 km shortening inferred for the Pakistan Himalaya (DiPietro and Pogue, 2004) are correct, the Pamir have absorbed ~600–900 km of Cenozoic convergence (1800–2100 – 300–700 – 200 = 600–900). This is ~55–64% shortening, two to three times that of Tibet (Fig. 2B–D).

Shortening in the Pamir might have produced enough crustal thickening (Fig. 2C and D) to drive large-scale lateral extrusion (e.g., Ratschbacher et al., 1991), exhumation by erosion/tectonic denudation, or recycling into the mantle (Negredo et al., 2007). If so, the high-grade rocks of the Pamir might be Cenozoic and might have been exhumed from quite deep crustal levels. Alternatively, the pre-Cenozoic crustal thickness of the Pamir might have been just 25–30 km (Burtman and Molnar, 1993), in which case the present-day 70 km-thick crust of the Pamir could have been built by homogeneous plane-strain vertical thickening with 55–64% shortening (Fig. 2B). In this scenario, the high-grade rocks of the Pamir might be dominantly pre-Cenozoic and only weakly exhumed.

* Corresponding author.

E-mail address: hacker@geol.ucsb.edu (B.R. Hacker).

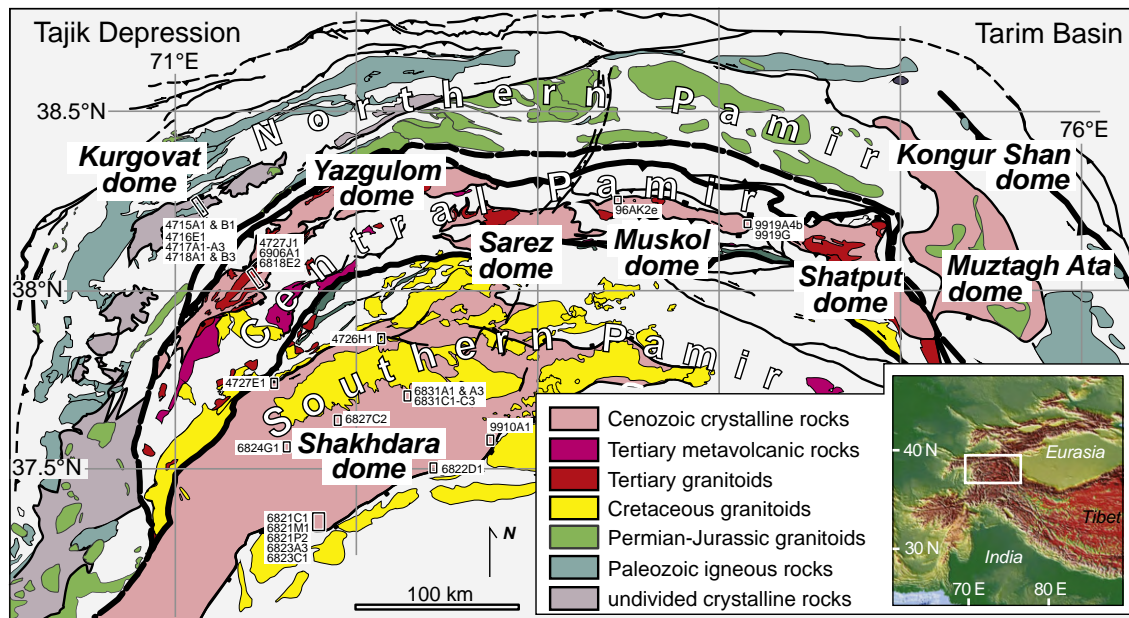


Fig. 1. Geology of the Pamir, emphasizing Cenozoic crystalline basement domes (pink) and Phanerozoic magmatic rocks; compiled from maps by Vlasov et al. (1991), Schwab et al. (2004), Doebrich and Wahl (2006), Robinson et al. (2007), and our own work from 1996–2011. Inset shows location of Pamir within India–Asia collision zone.

This contribution quantifies the exhumation depths of Pamir high-grade rocks using metamorphic petrology and provides new metamorphic age constraints with zircon, titanite and monazite geochronology. In conjunction with published work, we find that the high-grade crystalline rocks throughout the central and southern Pamir record 30–40 km of Oligo–Miocene burial and exhumation. In light of recent studies of xenoliths and seismological imaging, this record suggests that significant amounts of Pamir crust may have been recycled into the mantle. This is a tectonic history very different from that of Tibet.

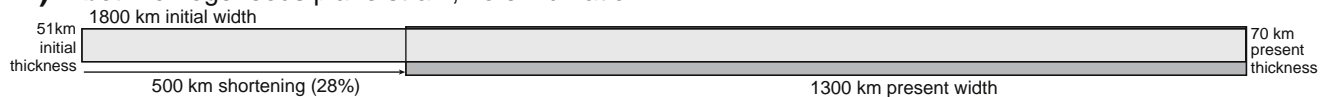
2. High-grade domes of the Pamir

Like Tibet, the Pamir are composed of a sequence of broadly E–W trending belts (Fig. 1) formed by successive collisions during the Late

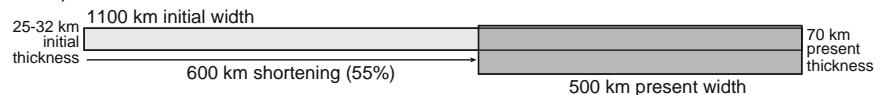
Paleozoic–Mesozoic (Schwab et al., 2004). The northern Pamir are a Paleozoic arc and subduction–accretion complex like the Kunlun and Hoh Xil–Songpan–Ganzi terranes of northern Tibet, the central Pamir comprise Paleozoic–Jurassic platform rocks correlative with the Qiangtang block, and the southern Pamir consist of Proterozoic gneiss, Paleozoic–Mesozoic metasedimentary rock, and Cretaceous–Paleogene granitoids equivalent to the Lhasa block (Schwab et al., 2004; Vlasov et al., 1991) or the Qiangtang block (Burtman, 2010; Robinson, 2009) in Tibet. Unlike Tibet, these belts have been bent into an arcuate shape and translated ~300 km northward over the Tajik Depression (Burtman and Molnar, 1993).

Each of the three major belts of the Pamir includes elongate culminations or domes of medium- to high-grade metamorphic rocks that collectively make up ~20% of the rock exposed in the Pamir (Fig. 1).

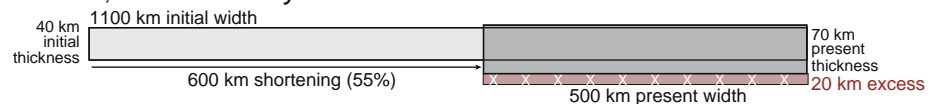
A) Tibet: homogeneous plane strain, no exhumation



B) Pamir: 600 km shortening of thin crust; no excess crustal material



C) Pamir: 600 km shortening of normal crust; 20 km-thick layer of excess crust



D) Pamir: 900 km shortening of normal crust; 40 km-thick layer of excess crust

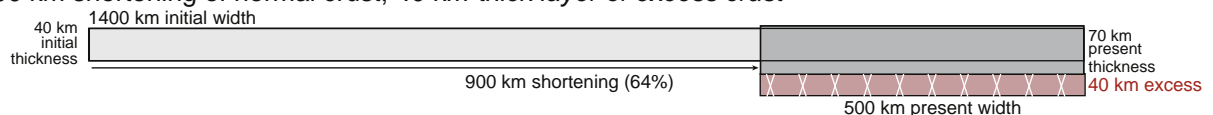


Fig. 2. Cenozoic exhumation of the Pamir domes from depths of 30–40 km can be explained by inhomogeneous shortening in a narrow zone. A) India–Asia convergence in Tibet can be explained by homogeneous plane strain. B) 600 km of homogeneous shortening of thin crust does not produce excess crustal material by thickening. C) 600 km of homogeneous shortening of normal-thickness crust produces 20 km of excess crust by thickening. D) 900 km of homogeneous shortening of normal-thickness crust produces 40 km of excess crust by thickening. (Crustal configuration before shortening in pale gray and crustal configuration after shortening in dark gray. Pink material removed by tectonic/erosional processes; shown at bottom of crust for convenience, but a component might also be removed from the top.)

Table 1
Thermobarometry samples.

Sample	Assemblage ^a	grt radius (μm)	grt resorption (μm)	N latitude	E longitude
<i>Kurgovat Dome</i>					
4715A1	grt bt st ms pl qtz	217	7	38°24.597'	71°06.487'
4715B1	grt ^b bt st ms pl qtz	1065	450	38°23.996'	71°08.193'
4716E1	grt ^b bt st ms pl qtz ilm	964	0	38°26.536'	71°01.380'
4717A1	grt bt hbl pl qtz ttn	283	3	38°23.299'	71°09.804
4717A3	grt ^b bt st ms pl qtz	2475	690	38°23.299'	71°09.804
4718A1	grt ^b bt st ms pl qtz ilm	1500	28	38°19.373'	71°13.475
4718B3	grt bt st ms pl qtz	1100	0	38°19.021'	71°16.658
<i>Yazgulom Dome</i>					
6906A3	grt bt st and pl qtz	550	100	37°58.009'	71°29.784'
<i>Muskol Dome</i>					
9919A4b	grt ^b bt ms pl qtz ttn	738	0	38°21.253'	74°26.563'
9919G6	grt bt ky ms pl qtz	1786	225	38°18.922'	74°26.320'
<i>Shakh dara Dome</i>					
4727E1	grt bt sil ms pl qtz	602	25	37°29.431'	71°31.816'
6821C1	grt ^b cpx hbl bt pl qtz ttn	600	106	36°46.516'	71°49.841'
6821M1	grt bt hbl pl qtz ttn	318	50	36°46.516'	71°49.841'
6821P2	grt cpx hbl bt pl qtz ttn	448	37	36°46.077'	71°51.238'
6822D1	grt bt ky sil pl qtz	986	155	37°00.299'	72°27.266'
6824G1	grt bt sil pl qtz rt	266	22	37°04.006'	71°32.337'
6827C2	grt bt sil ^c pl qtz rt	731	35	37°11.647'	71°51.842'
6831A1	grt bt sil ^c ms kfs pl qtz	500	35	37°13.466'	72°07.206'
6831C1	grt ^b bt sil ^c pl kfs qtz ttn	3850	0	37°14.504'	72°11.363'
6831C2	grt ^b bt ms ky pl qtz rt	3716	37	37°14.504'	72°11.363'

^a Mineral abbreviations after Kretz (1983).

^b Indicates zoned garnet.

^c Indicates kyanite interpreted as peak aluminosilicate.

These domes have surface areas of 10's to 100's of square kilometers, providing substantial windows into processes occurring deep within the crust during orogenesis and plateau formation. The domes are dominated by siliciclastic and carbonate metasedimentary sequences, but also include large volumes of quartzofeldspathic orthogneiss and granitoids as young as Tertiary (Schwab et al., 2004). The metamorphic mineral assemblages and textures in the domes indicate typical Barrovian facies-series metamorphism (culminating in kyanite + garnet + biotite with local migmatites) during N–S contraction. This was followed by syn-tectonic sillimanite or post-tectonic andalusite growth accompanied by plutonism and N–S stretching (Pashkov and Dmitriyev, 1981; Peykre et al., 1981; Robinson et al., 2004, 2007 and our observations).

Recent investigations have begun to quantify the exhumation depths and metamorphic ages of the domes. Robinson et al. (2007) demonstrated that the 16–8 Ma metamorphic rocks that core the Muztagh Ata dome were exhumed from depths of ~30–35 km to biotite closure to Ar loss by ~8 Ma, and Robinson et al. (2004, 2010) showed that similar 9 Ma metamorphic rocks that core the Kongur Shan dome were exhumed to biotite closure at ~1 Ma. On the opposite, western side of the Pamir, rocks in the western Shakh dara dome were metamorphosed at ~650 °C and > 25 km (Grew et al., 1994) and exhumed to Ar closure in biotite at 10–9 Ma (Hubbard et al., 1999).

3. Pressure–temperature conditions

We quantified the peak metamorphic conditions in the Kurgovat, Yazgulom, Muskol, and Shakh dara domes (see Fig. 1 and Table 1 for sample locations and parageneses). Optical microscopy was used first to assess phase relations and select specific grains for further analysis. X-ray maps of major-element concentrations in multiple phases in each sample were then made to assess phase zoning, infer growth and alteration histories, and to determine locations for quantitative compositional profiles. Mineral compositions were measured by wavelength-dispersive spectrometry on a Cameca SX-50 electron microprobe using a 2 μm spot, a 15 kV accelerating voltage and a 15 nA sample current, with natural and

synthetic standards (Appendix Table 1). Mineral formulae and endmember activities were calculated using the AX program of Holland (<http://wserv2.esc.cam.ac.uk/research/research-groups/holland/ax>).

Pressures and temperatures were calculated using the Holland and Powell (1998) thermodynamic dataset and THERMOCALC 3.26, using “mode 1” to calculate intersections of pairs of equilibria and “mode 2” to calculate intersections of multiple reactions (Table 2). Temperatures were derived chiefly from Fe–Mg exchange equilibria: garnet–biotite (GAR, Ferry and Spear, 1978), garnet–clinopyroxene (GC, Ellis and Green, 1979) and garnet–hornblende (GH, Graham and Powell, 1984), and pressures from the net-transfer reactions plagioclase–garnet–Al₂SiO₅–quartz (GASP, Ghent, 1976), biotite–plagioclase–garnet–muscovite (GBMP, Ghent and Stout, 1981), garnet–hornblende–plagioclase–quartz (GHPQ, Kohn and Spear, 1990) and garnet–plagioclase–clinopyroxene–quartz (GADS, Newton and Perkins, 1982). The pressures and temperatures calculated from phase compositions were checked against mineral parageneses in pseudosections calculated with *Perple_X* v. 7 (Connolly, 1990); see Appendix text and Appendix Fig. 1.

3.1. Northern Pamir Kurgovat dome

Rocks studied from the Kurgovat dome are dominantly garnet–staurolite–biotite schist with K-white mica (henceforth ‘muscovite’), plagioclase, quartz, and titanite. One mafic rock, 4717A1, contains post-tectonic hornblende garben in a matrix of fine-grained plagioclase and garnet + biotite + titanite + quartz (Fig. 3; Table 1). Garnet porphyroblasts are 0.5–5 mm in diameter, subidioblastic, and have strain shadows. The garnets in the metapelites have core compositions of alm_{65–80}prp_{08–11}grs_{06–17}sps_{03–19}¹ and rims of alm_{77–84}prp_{07–12}grs_{04–12}sps_{01–05}; garnets in 4717A1 have alm₆₃prp₁₄grs₁₀sps₁₃ cores and alm₆₃prp₁₂grs₁₀sps₁₆ rims. The garnets are characterized by two types of major-element zoning (Appendix Fig. 2). 1) Most have a bell-shaped Mn core–rim profile, with an abrupt increase at the rim; 4716E1 does

¹ alm, almandine; grs, grossular; prp, pyrope; sps, spessartine.

Table 2
Summary of pressure-temperature determinations.

Sample	THERMOCALC mode 1				THERMOCALC mode 2				Perple_X pseudosections				
	Method ^a	T (°C)	Method ^a	P (kbar)	Method ^b	T (°C)	Method ^b	P (kbar)	Fit	Corr	Excluded	T (°C)	P (kbar)
<i>Kurgovat</i>													
4715A1	GARB	569 ± 61	GBMP	7.6 ± 0.9	gbmpq	569 ± 58	gbmpq	7.6 ± 0.8	0.05	0.85	east	600–640	6.2–8.8
					gbmpqst	594 ± 53	gbmpqst	8.2 ± 0.9	1.42	0.74	east		
4715B1	GARB	582 ± 62	GBMP	7.1 ± 0.9	gbmpq	583 ± 59	gbmpq	7.1 ± 0.8	0.16	0.82	east	575–650	5–9
					gbmpqst	619 ± 40	gbmpqst	7.6 ± 0.7	0.81	0.69	east		
4716E1	GARB	537 ± 55	GBMP	6.0 ± 0.8	gbmpq	541 ± 56	gbmpq	6.0 ± 0.8	0.35	0.70	pa	Not definitive	
					gbmpqst	656 ± 82	gbmpqst	7.4 ± 1.3	1.56	0.58	pa		
4717A1	GH	648 ± 55	GHPQ	5.8 ± 0.9	ghpq	649 ± 55	ghpq	5.8 ± 0.9	0.07	0.57	east, parg	Not definitive	
4717A3	GARB	548 ± 57	GBMP	6.1 ± 0.8	gbmpq	575 ± 55	gbmpq	6.4 ± 0.8	0.59	0.76	–	560–680	5–8
					gbmpqst	638 ± 55	gbmpqst	7.3 ± 0.9	1.33	0.63	–		
4718A1	GARB	542 ± 56	GBMP	5.5 ± 0.7	gbmpq	542 ± 58	gbmpq	5.5 ± 0.7	0.06	0.81	cel, pa	570–630	5–6.5
					gbmpqst	626 ± 68	gbmpqst	6.5 ± 0.9	1.36	0.70	cel, pa		
4718B3	GARB	560 ± 59	GBMP	6.2 ± 0.8	gbmpq	560 ± 57	gbmpq	6.2 ± 0.8	0.17	0.77	–	570–655	5–7.8
					gbmpqst	638 ± 52	gbmpqst	7.2 ± 0.8	1.21	0.62	–		
<i>Yazgulom</i>													
6906A3	GARB	597 ± 61	GASP‡	9.7 ± 0.7	gbpqk	588 ± 60	gbpqk	9.4 ± 1.3	0.27	0.88	–	610–650	7–9
<i>Muskol-Sares</i>													
9919A4b					gbmp	776 ± 83	gbmp	10.5 ± 1.2	0.87	0.91	–	Not definitive	
					Assembl.	500–700	gbmpq	6.9–9.6(±0.07)	1.70	–	–		
9919G6	Assembl.	650–800	GASP‡	6.6–10.2(±0.6)	gbpqk	770 ± 96	gbpqk	11.2 ± 1.8	0.56	0.93	–	620–760	7–11
<i>Shakh dara</i>													
4727E1	GARB	703 ± 89	GASP	6.9 ± 1.1	gbpqs	672 ± 76	gbpqs	6.2 ± 1.0	0.50	0.66	east	620–730	5–9
6821 C1	GC	587 ± 56	GADS	7.2 ± 0.9	ghcpq	554 ± 59	ghcpq	6.9 ± 0.9	0.11	0.82	parg, fact, CaTs		
					Assembl.	700–750	ghcpq	8.7–9.4(±1.0)	1.70	–	parg, fact, CaTs	680–770	9–13
6821M1	GH	959 ± 125	GHPQ	11.3 ± 4.2	ghpq	950 ± 170	ghpq	9.7 ± 3.4	0.32	0.89	–	500–680	7–10.5
	Assembl.	600–700	GHPQ	8.5–9.3(±2.8)	Assembl.	600–700	ghpq	3.5–5.3(±2.0)	–	–	–		
6821P2	GC	675 ± 65	GADS	10.6 ± 1.2	ghcpq	678 ± 75	ghcpq	10.6 ± 1.2	0.15	0.90	parg, fact, CaTs	Not definitive	
6822D1	GARB	762 ± 78	GASP‡	9.1 ± 0.6	gbpqk	792 ± 85	gbpqk	9.5 ± 1.5	0.70	0.90	–	not definitive	
	Assembl.	700–800	GASP‡	8.2–9.7(±0.6)							–		
6824G1	Assembl.	700–800	GASP‡	6.3–7.5(±0.8)	gbpqs	720 ± 85	gbpqs	6.5 ± 1.7	0.20	0.65	–	700–740	6.8–8.5
6827C2	Assembl.	700–800	GASP‡	8.1–9.6(±0.6)	gbpqs	670 ± 62	gbpqs	7.7 ± 1.1	0.02	0.77	–	625–800	6–10
6831A1	Assembl.	700–800	GASP‡	8.5–10.1(±0.7)							–	720–775	8–12
6831C1	Assembl.	700–800	GASP‡	12.6–14.6(±0.4)							–	Not definitive	
6831C2	GARB	770 ± 74	GASP‡	9.4 ± 0.5	gbpqk	755 ± 75	gbpqk	9.1 ± 1.2	0.42	0.85	–	610–720	8–11
	Assembl.	700–800	GASP‡	8.3–9.8(±0.5)							–		

Preferred pressure and temperature in bold face. “Assembl.” indicates qualitative temperature determined from mineral assemblage.

^a Uppercase letters indicate a single equilibrium was used to determine P or T:

GARB, garnet–biotite; GH, garnet–hornblende; GC, garnet–clinopyroxene; GBMP, garnet–biotite–muscovite–plagioclase.

GASP, garnet–aluminum silicate–quartz–plagioclase; GADS, garnet–plagioclase–clinopyroxene–quartz; GHPQ, garnet–hornblende–plagioclase–quartz.

^b Lowercase letters indicate that all equilibria among the named phases were used:

g, garnet; b, biotite; m, muscovite; p, plagioclase; q, quartz; st, staurolite; h, amphibole; c, clinopyroxene; k, kyanite; s, sillimanite.

‡ kyanite was used as peak phase.

“fit”, fit parameter from THERMOCALC.

“corr”, correlation in ± P and ± T from THERMOCALC.

“excluded”, end-member activities excluded from fit (east, eastonite; parg, pargasite; pa, paragonite; cel, celadonite; CaTs, Ca–Tschermak pyroxene; fact, ferroactinolite).

not have a Mn-enriched rim. The Mg# increases outward from the core, except in the Mn-enriched rims, where it decreases. Ca decreases from core to rim. 2) Garnets in three samples (4715A1, 4717A1 and 4718B3) have homogeneous Mn, Mg, and Fe concentrations in their cores. Of these, samples 4715A1 and 4717A1 display an abrupt increase in Mn and decrease in Mg# at the rim, whereas 4718B3 is homogeneous throughout. 4715A1 also has a bell-shaped Ca distribution, whereas 4717A1 is homogeneous in Ca. Plagioclase varies from An₁₈–An₄₀ among the samples; the anorthite component decreases concentrically from An₃₂ to An₂₉ in 4715A1, whereas all other samples have patchy zoning. Muscovite is generally 200–400 μm; it is a foliation-forming mineral in samples 4715B1, 4717A3, and 4718B3, whereas in 4715A1, 4716E1, and 4718A1, it is a minor decussate, post-kinematic phase. Muscovite has K/K + Na ratios of 70–85, 3.0–3.1 Si atoms per formula unit (pfu), 0.3–0.5 wt.% TiO₂, and Mg#45–65. Staurolite porphyroblasts

are either small (~600 μm), xenoblastic, partially resorbed, and have undulatory extinction, or are large (~5 mm) idioblastic, and decussate; they generally display outward zoning from Mg#20 to 16. Biotite in the metapelites are Mg#47–53, and in the amphibolite they are Mg#56–59. In most samples (4715A1, 4715B1, 4716E1, 4718B3) biotite decreases in Mg# with increasing distance from garnet; the remaining samples exhibit no trend. Amphibole in sample 4717A1 is ferropargasite and has concentric zoning with 1.2–2.1 wt.% Na₂O, 0.1–0.4 wt.% TiO₂, and 6.1–6.5 Si atoms pfu.

Major-element zoning was used as an indicator of whether the garnets preserve prograde compositions or were modified by diffusion and/or retrogression. Bell-shaped Mn profiles were considered characteristic of prograde growth (Hollister, 1966). Mn increases at the garnet rims were interpreted to reflect resorption (Kohn and Spear, 2000); such grains also have subidioblastic habits compatible with resorption. Garnets

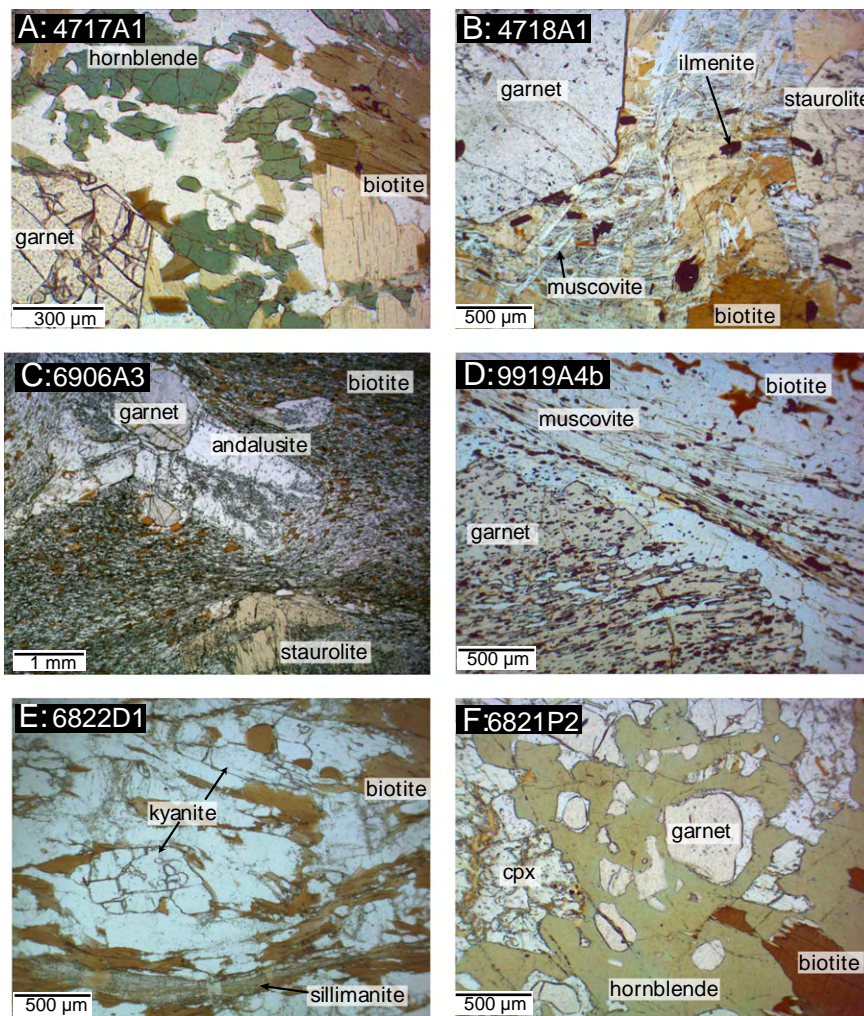


Fig. 3. Photomicrographs of representative Pamir dome samples. (A) Kurgovat garnet-biotite amphibolite with idioblastic garnet; (B) Kurgovat metapelite with idioblastic garnet; (C) Yazgulom metapelite with late andalusite; (D) Muskol metapelite; (E) Shakh dara metapelite with peak kyanite and late sillimanite in shear bands; (F) Shakh dara clinopyroxene-garnet amphibolite.

with Ca zoning and homogeneous Mg, Fe, and Mn were assumed to have undergone partial diffusional homogenization (Yardley, 1977).

The method of Kohn and Spear (2000) was used to determine the magnitude of garnet resorption, to estimate the composition of garnet rims prior to resorption, and to correct biotite compositions for the net transfer of Fe and Mg from garnet to biotite. The decrease in Mg# of biotites increasingly distant from garnet was also used as a measure of the effects of garnet resorption on biotite composition. The magnitude of resorption was calculated to be as much as 30% of the garnet diameter (Table 1).

To calculate pressures and temperatures (Table 2), we used the recalculated rim compositions of resorbed garnets with bell-shaped Mn profiles and the core compositions of homogeneous garnets, along with the core compositions of staurolite, muscovite, plagioclase, and biotite distant from garnet. This biotite composition was either identical to the net-transfer-corrected composition of biotite adjacent to garnet or gave a lower MSWD (mean square of weighted deviates, a measure of goodness of fit) in THERMOCALC, leading to the conclusion that such grains were least affected by garnet resorption and best represent peak conditions. Where available, plagioclase inclusions in homogeneous garnets were used to calculate pressure.

The presence of staurolite + garnet + biotite in the Kurgovat rocks implies temperatures of ~500–650 °C. Metamorphic temperatures and pressures calculated using the intersections of GARB and GBMP (i.e., mode 1) or THERMOCALC mode 2 (excluding staurolite), are

540–650 °C and 5.5–7.6 kbar (Fig. 4). When staurolite is included, mode 2 results are slightly higher: 600–650 °C at 6.5–8.2 kbar. Calculations for the amphibolite, based on GH and GHPQ, yielded 649 ± 50 °C and 5.8 ± 0.9 kbar. Pseudosections calculated with *Perple_X* are compatible with these results.

3.2. Central Pamir Yazgulom dome

One sample from the orthogneiss-dominated Yazgulom dome is a garnet-andalusite-staurolite hornfels with biotite, plagioclase, and quartz (Fig. 3; Table 1). The garnet porphyroblasts are subidioblastic, ~1 mm in diameter, and have thin quartzofeldspathic haloes. Idioblastic staurolite porphyroblasts are ~5 mm long and co-genetic with garnet; both have muscovite- and biotite-filled strain shadows. Andalusite is ~4 mm long, idioblastic and sector zoned. Biotite is the main foliation-forming phase, and ~60 µm long, except for a few ~500 µm grains in garnet strain shadows and cracks. The garnets have bell-shaped Mn profiles with an abrupt increase in the outer 40 µm. Mg# increases outward, except in the outer 40 µm, where it decreases; Ca decreases slightly from core to rim. Garnet cores are $\text{alm}_{70}\text{prp}_{06}\text{grs}_{09}\text{sps}_{15}$, and rims are $\text{alm}_{80}\text{prp}_{11}\text{grs}_{07}\text{sps}_{02}$. The larger biotite grains have concentric core-rim zoning from Mg#45 to 43. Staurolite grains are Mg#18.

We followed the same logic detailed for the Kurgovat dome when calculating pressure-temperature conditions for the Yazgulom sample, using resorption-corrected garnet and biotite rim compositions

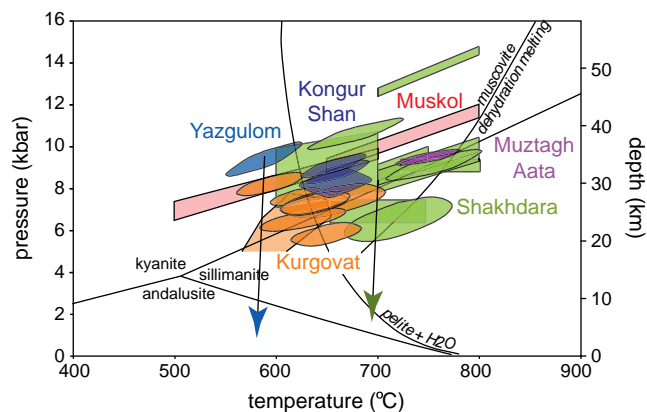


Fig. 4. Metamorphic pressures and temperatures indicate that the Pamir domes were exhumed from lower crustal depths of 30–40 km. Arrows reflect observed and inferred decompression. Solidi from Vielzeuf and Schmidt (2001).

with plagioclase rims. THERMOCALC mode 2 indicates 588 ± 60 °C and 9.4 ± 1.3 kbar (Fig. 4), indistinguishable from the mode 1 GASP–GARB intersection. *Perple_X* returned compatible results. The calculated pressure is well above the stability field of andalusite, suggesting that the andalusite replaced kyanite.

3.3. Central Pamir Muskol dome

Two samples were analyzed from the eastern part of the Muskol dome. One (9919 G6) is a garnet–kyanite–biotite schist with muscovite, plagioclase, and quartz. The garnet is minor, hypidioblastic, and ~3.5 mm in diameter. It has a core of $\text{alm}_{79}\text{prp}_{13}\text{grs}_{05}\text{sps}_{02}$ and a rim of $\text{alm}_{77}\text{prp}_{14}\text{grs}_{03}\text{sps}_{06}$. It displays a dish-shaped Mg# profile except in the outer 120 μm , where Mg decreases and Mn increases; Ca decreases outward. Kyanite porphyroblasts are ~1 mm, hypidioblastic and aligned parallel to the lineation. Plagioclase displays patchy recrystallization in the range An_{12-19} . Biotite is 500–1000 μm long and generally tabular, with compositions of Mg#37–39 that do not vary systematically with texture.

The second Muskol sample (9919A4b; Fig. 3) is a garnet–biotite schist with muscovite, plagioclase, quartz, and rare staurolite inclusions in garnet. The garnet porphyroblasts are 1–2 mm, xenoblastic, and typically elongate; they have dish-shaped Mg# profiles with cores of $\text{alm}_{84}\text{prp}_{04}\text{grs}_{12}\text{sps}_{00}$ and rims of $\text{alm}_{73}\text{prp}_{10}\text{grs}_{18}\text{sps}_{00}$. The more-equant garnets have a Ca spike in the outer 10% of the grain. Biotite and muscovite are 200–400 μm and aligned parallel to the foliation; large biotite decrease in Mg#36–34 from core to rim. Muscovite has Mg#48–59, 0.3–1.0 wt% TiO_2 , 3.1 Si atoms pfu, and K/K + Na of 93–94.

For sample 9919 G6, with homogeneous garnet, mineral cores were used to determine metamorphic P–T conditions. For sample 9919A4b, garnet has a bell-shaped Mn profile, so mineral rims were used to calculate the pressure–temperature conditions. In both cases, the temperature given by GARB is in excess of the probable mineral-stability conditions. At 500–700 °C, the samples give mode 2 pressures of 6.6–10.2 kbar and 6.9–9.6 kbar, respectively (Fig. 4); *Perple_X* returned compatible results for 9919G6.

3.4. Southwestern Pamir Shakhhdara dome

Two types of samples were collected from the Shakhhdara dome (Fig. 3; Table 1). Seven are garnet–sillimanite–biotite \pm kyanite schist with plagioclase + quartz \pm muscovite \pm K-feldspar \pm titanite \pm rutile. Three samples are garnet amphibolite that contain biotite + plagioclase + quartz + titanite \pm clinopyroxene; leucocratic layers in outcrop suggest partial melting.

The garnets are hypidioblastic porphyroblasts, 0.4–15 mm in diameter. All the metapelites contain sillimanite along late shear

bands that cut the foliation, except 6831C2, in which kyanite included in garnet is the only aluminosilicate. Sample 6822D1 contains kyanite as a matrix phase, in addition to the sillimanite. The metapelitic garnets have cores of $\text{alm}_{50-79}\text{prp}_{09-27}\text{grs}_{02-10}\text{sps}_{02-09}$ and rims of $\text{alm}_{59-79}\text{prp}_{06-28}\text{grs}_{02-12}\text{sps}_{02-15}$, whereas the amphibolite garnets have core and rims of $\text{alm}_{51-61}\text{prp}_{06-12}\text{grs}_{31-35}\text{sps}_{02-03}$ and $\text{alm}_{53-63}\text{prp}_{05-12}\text{grs}_{29-33}\text{sps}_{03-05}$, respectively. Most of the metapelite garnets have cores that are homogeneous in Mn and Mg, with abrupt increases in Mn and decreases in Mg in the outer <30% of the grain. Ca decreases from core to rim, except in three samples, in which it is homogeneous. Two of these samples (6831C1 and 6831C2) exhibit broad increases in Mg# from core to rim. 6831C2 displays a rim spike in Mn and drop in Mg# in the outer 5% of the grain. The amphibolite garnets are homogeneous in Mn and Mg, except for abrupt increases in Mn and decreases in Mg in their outer 12–25%; garnet in 6821C1 also exhibits a broad increase in Mg out to the rim, where it drops. Ca decreases broadly rimward.

Plagioclase is a xenoblastic matrix phase in most of the metapelites, but also forms rare inclusions in garnet; most are An_{11-35} and have patchy zoning. Two samples however, have plagioclase zoned outward from An_{21} to An_{26} , and plagioclase in sample 4727E1 is zoned rimward from An_{23} to An_{15} . Rare (<5%) tabular muscovite in 4727E1 is aligned parallel to the foliation, has 3.0 Si atoms pfu, 1.3–1.5 wt% TiO_2 , a K/K + Na ratio of 88–90, and Mg#40–44. Biotite is chiefly a matrix phase, but also occurs in shear bands, in garnet strain shadows, and as a rare inclusion in garnet. Matrix biotite typically ranges from Mg#41 to 58, except in 4727E1, where it is Mg#27–30; zoning is typically not systematic.

Clinopyroxene in samples 6821 C1 and 6821P2 is xenoblastic and exhibits patchy zoning of Mg#63–70, 1.0–3.5 wt% Al_2O_3 , and 0.3–1.0 wt% Na_2O . Hornblende is ferropargasite and has 6.1–6.3 Si atoms pfu, 1.1–2.0 wt% TiO_2 , and 1.1–1.5 wt% Na_2O . An_{17-53} plagioclase in the garnet amphibolites is xenoblastic and displays patchy zoning; 6821 M1 includes minor antiperthite.

For the bulk of the samples that have garnet cores that are homogeneous in Mn and Mg, the core garnet, biotite, and plagioclase compositions were used to calculate temperature and pressure. The exception is sample 6831C2, which has garnets with bell-shaped Mn profiles, for which the resorption-corrected garnet rim composition was used, along with the rim compositions of biotite and plagioclase.

Most of the Shakhhdara metapelites give calculated mode 2 temperatures and pressures of 670–800 °C and 6.2–9.9 kbar. Samples 6831A1 and 6831C1 contain so little biotite (<3 vol%), that calculation of their pre-resorption compositions was deemed unreliable, and temperatures of 700–800 °C were estimated from their mineral assemblages instead. For these two samples the GASP reaction gives pressures of 8.5–14.6 kbar. GASP–GARB intersections for the remainder of the metapelites yield temperatures of 700–800 °C and pressures of 6.9–9.7 kbar. The clinopyroxene-bearing samples yield mode 2 temperatures and pressures of 554–680 °C and 6.9–10.6 kbar; the GADS–GC intersections are 587–676 °C and 7.2–10.6 kbar. Mafic sample 6821 M1, which lacks clinopyroxene, gave mode 2 temperatures of >900 °C—far beyond the probable stability field of the mineral assemblage; at 600–700 °C the GHPQ barometer yields pressures of 8.5–9.3 kbar (Fig. 4). *Perple_X* returned compatible results for all samples.

4. Age of metamorphism

There is considerable uncertainty in the older literature about the age of the metamorphic events in the Pamir domes, with suggestions of Proterozoic to Alpine tectonism hinging on the interpretation of unclear field relations (Pashkov and Dmitriyev, 1981; Peykre et al., 1981). Limited radiochronology has documented Mesozoic through Miocene metamorphism (Hubbard et al., 1999; Robinson et al., 2004; Robinson et al., 2007; Schwab et al., 2004; Stübner et al.,

2011), but there are relatively few ages from the high-grade domes. Th-Pb monazite ages indicate Barrovian metamorphism of the north-eastern Pamir Kongur Shan and Muztaghata domes between 24 Ma and 7 Ma, and biotite $^{40}\text{Ar}/^{39}\text{Ar}$ ages indicate exhumation to upper crustal levels by 8 Ma at Muztagh Ata (Robinson et al., 2007) and at 1 Ma in the Kongur Shan (Robinson et al., 2010). On the opposite, western, side of the Pamir, rocks in the Shakh dara dome have biotite $^{40}\text{Ar}/^{39}\text{Ar}$ ages of 18–9 Ma (Hubbard et al., 1999).

We performed reconnaissance assessment of the metamorphic ages of the Kurgovat, Yazgulom, Muskol, and Shakh dara domes (Fig. 1; Appendix text and Table 2) using U/Th-Pb ages of zircon, monazite, and titanite; multiple grains, and multiple spots within some grains, were analyzed in each sample. The analyses were conducted by secondary-ion mass spectrometry (SIMS) at UCLA (following Robinson et al., 2004) and St Petersburg (see Appendix for analytical details), laser-ablation multi-collector inductively coupled plasma mass spectrometry (LA-MCICPMS) at the University of Arizona (following Hacker et al., 2006) and UCSB (see Appendix for analytical details). All quoted uncertainties are 2σ and include contributions from the external reproducibility of the primary reference material. U-Pb data presentation employed Isoplot (Ludwig, 2003).

4.1. Kurgovat dome

Metamorphic rocks in the Kurgovat dome have been mapped as Proterozoic with a Carboniferous–Permian cover (Vlasov et al., 1991). We obtained exclusively concordant, Mesozoic $^{206}\text{Pb}/^{238}\text{U}$ and $^{208}\text{Pb}/^{232}\text{Th}$ ages of 210–195 Ma from monazite in a garnet–two mica schist (sample 4717A2 in Fig. 5).

4.2. Muskol dome

In four Pamir samples we analyzed titanite with textures that indicate an unambiguous association with metamorphism and deformation. In each case the titanite formed from the breakdown of ilmenite \pm biotite \pm plagioclase and underwent polygonization during deformation (Fig. 5). Multiple titanites from one of those samples—a tonalitic gneiss (96Ak2) in the Muskol dome—yielded a U-Pb age of 16.7 ± 0.3 Ma (Fig. 5).

4.3. Yazgulom dome

Similarly textured titanite from a dioritic gneiss (6906A1) in the Yazgulom dome gave a U-Pb intercept age of 19.1 ± 0.4 Ma (Fig. 5). Zircons in a coarse-grained, weakly deformed leucocratic dike (4727J1) have inherited components as old as 2.5 Ga that are overgrown by euhedral oscillatory zoned portions with Th/U ratios of 0.6–1.0 and $^{206}\text{Pb}/^{238}\text{U}$ ages as young as 21.2 ± 0.3 Ma. A second, weakly deformed leucogranite (6818E2) from the northern shear zone of the Yazgulom dome has monazite that gave $^{208}\text{Pb}/^{232}\text{Th}$ ages ranging from ~22 to 19 Ma.

4.4. Shakh dara dome

The giant Shakh dara dome has relict Early Proterozoic basement and ubiquitous Cretaceous orthogneiss and granitoid (Schwab et al., 2004). The oldest Cenozoic ages we obtained from the Shakh dara dome are 30–18 Ma monazite ages from paragneiss (9910A1). Two other monazite samples from Shakh dara gave ages toward the younger end of that range. A strongly deformed leucocratic gneiss with a recrystallized metamorphic mineral assemblage (6823A3) has a mean $^{208}\text{Pb}/^{232}\text{Th}$ age of 21.1 ± 0.7 Ma, and a paragneiss (6831A3) from the same locality of petrology sample 6831A1 (and nearby to 6831C) yielded a mean $^{208}\text{Pb}/^{232}\text{Th}$ age of 22.1 ± 0.3 Ma. A gneissic pegmatite from the northern Shakh dara dome (4726H1) is almost identical to dike 4727J1 from the Yazgulom dome: it has inherited

zircons as old as 2.5 Ga and ~29 Ma high-Th/U zircons overgrown by low-Th/U, oscillatory zoned zircon as young as 20.5 Ma. The youngest zircons in a weakly deformed post-metamorphic aplite dike (6831C3) are 12.0 ± 0.4 Ma. The sample is from the same locality of petrology samples 6831C1 and 6831C2. Metamorphic titanite from gabbroic gneiss (6823C1) gave a U-Pb age of 10.1 ± 0.2 Ma.

5. Discussion

5.1. Pressure–temperature conditions

The relatively simple mineralogy and phase zoning of the samples examined in this study allows reasonably straightforward interpretation of equilibrium compositions and the calculation of P-T conditions (Fig. 4). The pressure–temperature conditions of the Kurgovat dome peaked at 600–650 °C and 6.5–8.2 kbar, consonant with the stability of garnet + staurolite + biotite. The hornfelsic texture and the presence of andalusite are in conflict with the calculated GASP pressure of 9.4 ± 1.3 kbar for the Yazgulom sample, however, suggesting that the andalusite overprints an earlier higher pressure metamorphism recorded in the plagioclase and garnet. Robinson et al. (2004) reported similar mineral parageneses from the northern hanging wall of the Kongur Shan dome, and inferred peak metamorphic conditions of 650–700 °C and 4–5 kbar.

Using the data of Robinson et al. (2004, 2007), we calculate pressures and temperatures of 8–9 kbar and 650 °C for Cenozoic metamorphism in the footwall of the Kongur Shan dome, and 9 kbar and 750 °C for Muztagh Ata. The pressure–temperature estimates for the two metapelites from the Muskol dome are broadly similar: 6.9–11.7 kbar and 500–800 °C. Pressure–temperature estimates for the Shakh dara dome metapelites range from 6.5 ± 1.7 kbar and 720 ± 85 °C to 13.6 ± 1.0 kbar and 750 ± 50 °C. The highest pressures are consonant with the presence of kyanite in some samples, but the presence of sillimanite in shear bands implies continued recrystallization during decompression. Decompression during heating (from ~650 °C and >7 kbar to 650–750 °C and <4 kbar) has been inferred for ultra-magnesian rocks in the western Shakh dara dome by Grew et al. (1994).

Using a density of 2800 kg/m³, the maximum exhumation depth of all the studied Pamir domes is ~30–40 km. At least two domes show mineralogical evidence of decompression to upper crustal depths of 14–18 km with little loss of heat, compatible with rapid exhumation and/or exhumation accompanied by plutonism.

5.2. Ages

Our preliminary radiochronology, in conjunction with that of other workers, documents that the bulk of the deep crust exposed in the central and southern Pamir was last metamorphosed in the Oligo–Miocene, although there are local records of earlier events. The 210–195 Ma monazite ages from the Kurgovat dome are similar to the 234–192 Ma monazite ages reported for the hanging wall of the Kongur Shan dome (Robinson et al., 2004); all are part of broader Triassic–Jurassic orogenic activity that extended across Asia (Roger et al., 2008; Schwab et al., 2004). In light of the Carboniferous–Permian depositional age of the Kurgovat dome metasedimentary rocks, Permo–Triassic burial is required. If peak temperatures in the Kurgovat dome were indeed <700 °C (Fig. 4), it is likely that the monazite ages record the time of prograde metamorphism (closure to Pb diffusion is >900 °C for 10 μm grains cooled at 10 K/Myr, Cherniak and Pyle, 2008; Gerdes et al., 2007; McFarlane and Harrison, 2006).

The whole-grain closure temperature of the U-Pb system in titanite is >650 °C and probably >700 °C (Aleinikoff et al., 2002; Frost et al., 2000; Pidgeon et al., 1996; Scott and St-Onge, 1995). Our own experience with >150 multi-titanite U-Pb dates from Norwegian Barrovian facies-series quartzofeldspathic gneisses (Kylander-Clark et al., 2008; Spencer et al., 2010) is that the closure temperature is ~650 °C, but that titanite can

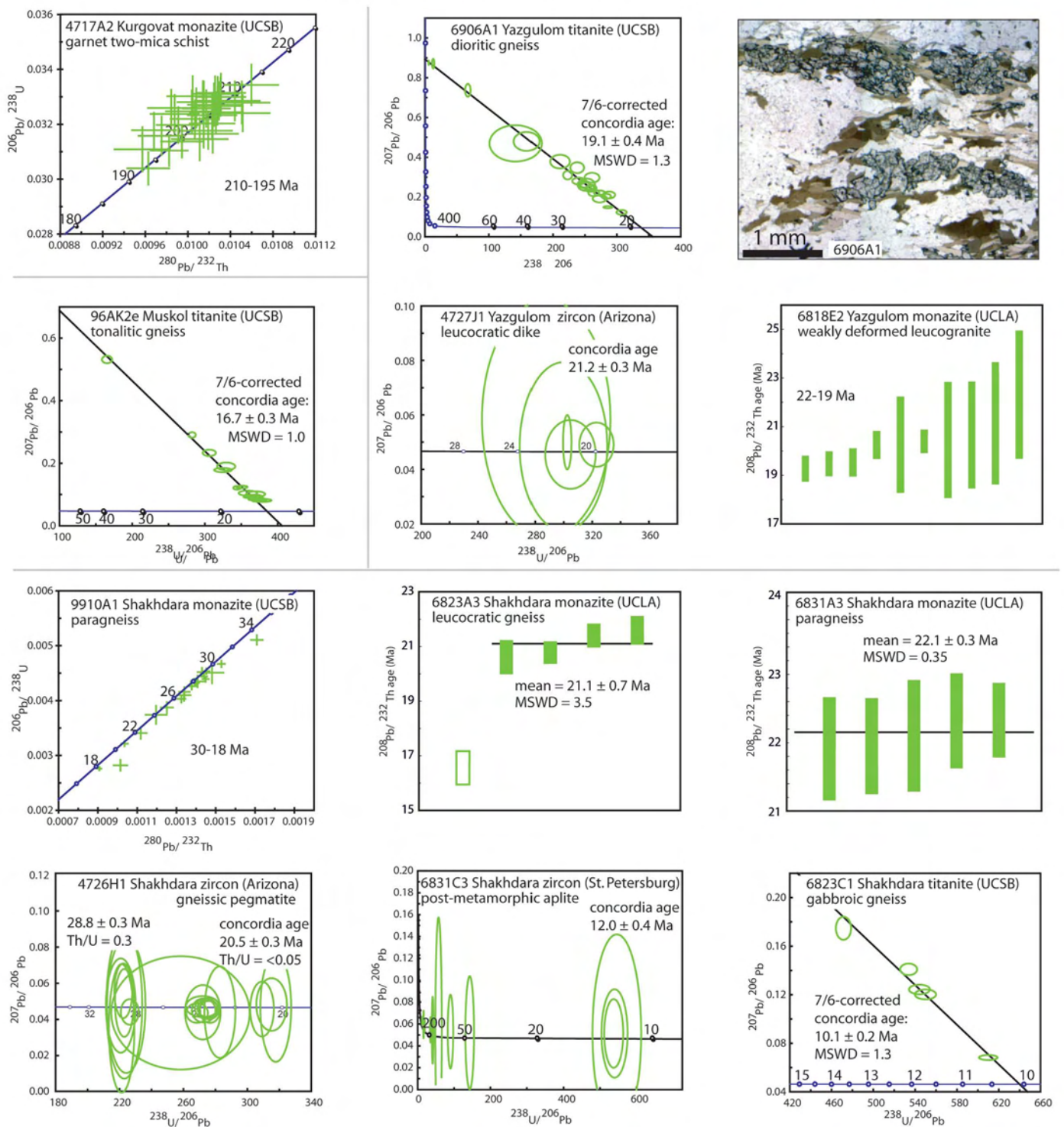


Fig. 5. Cenozoic ages from the Yazgulom, Muskol and Shakhudara domes and a Jurassic age from the Kurgovat dome. Zircon and titanite data shown on Tera-Wasserburg concordia; the titanite data are not corrected for common Pb. Monazite LA-MCICPMS data displayed as Th-Pb/U-Pb concordia, and monazite SIMS data shown as $^{208}\text{Pb}/^{232}\text{Th}$ ages. Uncertainties are 2σ . Numbers on concordia are ages in Ma. Note that because of the emphasis on the Cenozoic importance of these rocks, some older data are not plotted. Foliation-forming polycrystalline titanite grains in 6906A1 are shown in upper right.

effectively remain closed for at least 10 Myr at 800 °C; this is in accord with experiments (Cherniak, 1993) suggesting a closure temperature > 780 °C at the Myr timescale for 500 μm crystals. If so, the titanite ages from the Muskol and Yazgulom domes likely indicate prograde metamorphism and deformation (and thus, probably burial) at 16.7 and 19.1 Ma, respectively. Monazite and zircon in the Yazgulom dome indicate late-stage leucogranite crystallization at 22–19 Ma (Fig. 5).

The range of monazite, zircon, and titanite ages from the giant Shakhudara dome indicates that Cenozoic magmatism and metamorphism were underway by 30–29 Ma, and monazite ages of ~22 Ma from three separate locations imply continuing prograde metamorphism; zircon ages from a post-metamorphic aplite suggest that metamorphism terminated locally by 12 Ma. Deformed titanite with an age of 10 Ma may reflect local prograde recrystallization, but it is similar

enough to biotite $^{40}\text{Ar}/^{39}\text{Ar}$ ages of 10–9 Ma (Hubbard et al., 1999) it may instead reflect cooling-related closure.

Similar ages for Cenozoic metamorphism in the Muztagh Ata dome are indicated by 33–22 Ma ages from low-Th/U zircons, 30–8 Ma monazite matrix grains (mostly 15–8 Ma), and 8 Ma $^{40}\text{Ar}/^{39}\text{Ar}$ ages for biotite (Robinson et al., 2007). It is reasonable to associate the ~10 Ma transition in the Shakh dara and Muztagh Ata domes from high-grade metamorphism (zircon, monazite, titanite) to cooling (biotite) with exhumation, and this corresponds to the beginning of syn-orogenic coarse clastic sedimentation in the foreland basins, which are uppermost Miocene to Pliocene (Tajik depression and Pamir frontal range, Leonov, 1977; Schwab et al., 1980; and Tarim Basin, Jin et al., 2003). Exhumation in the Kongur Shan dome to biotite closure is even younger, ~1 Ma (Robinson et al., 2010).

5.3. Convergence and crustal recycling

Three aspects suggest that Pamir continental crust may still be being recycled into the mantle: intermediate-depth seismicity, crustal xenoliths, and the exhumation depths of the domes. The Pamir are underlain by intermediate-depth seismicity indicative of active subduction from the north and south. The south-dipping zone extends beneath the northern Pamir to a depth of 150 km and has been interpreted to be the result of intracontinental subduction, based on the absence of exposed ocean crust in the region (Burtman and Molnar, 1993; Hamburger et al., 1992). A north-dipping zone west of the Pamir beneath the Hindu Kush has been interpreted to mark ~700 km of subducted Indian lithosphere (Negredo et al., 2007), and slow velocities to at least 150 km depth are compatible with the subduction of continental crust (Roecker, 1982). In the Miocene, crustal xenoliths of Asian affinity were erupted from mantle depths of 90 km in the southeastern Pamir (Gordon et al., in review; Ducea et al., 2003; Hacker et al., 2005). Regardless of whether these xenoliths are the result of lower crustal foundering or subduction erosion (Hacker et al., 2011), they indicate definitively that Pamir crust was—and may still be—locally present at depths of 90 km, well below the present Moho.

As noted in the Introduction, the disparity in N–S dimensions of the Pamir and Tibet requires the Pamir to have undergone considerably more Cenozoic strain in response to India–Asia convergence: ~19–28% shortening in Tibet and 55–64% shortening in the Pamir (Fig. 2). (The oroclinal shape of the Pamir precludes major E–W shortening, so these plane-strain calculations are minima.) The Cenozoic deep exhumation of the Pamir crystalline domes documented here can be interpreted in the light of two endmember models that differ only in their pre-collisional crustal thickness (Fig. 6).

5.3.1. Model A

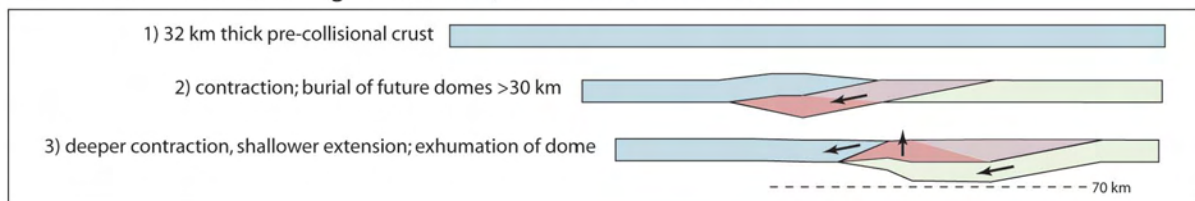
If the crust of the Pamir prior to the India–Asia collision was only 25–32 km thick — as inferred by Burtman and Molnar (1993) from a review of stratigraphic sections and seismic data from the Tajik Depression — the inferred 55–64% shortening of the Pamir could have been accommodated solely by homogeneous plane-strain vertical thickening (Fig. 6A). Each of the deeply exhumed Cenozoic Pamir domes must then represent a zone of unusually great exhumation, and each must be compensated by a corresponding zone of less exhumation.

5.3.2. Model B

Alternatively, the pre-Cenozoic Pamir crust might have been substantially thicker—e.g., 35–40 km as inferred for the southern Tian Shan (Bagdassarov et al., 2011), or, perhaps even locally 70 km thick as speculated for southern and central Tibet (Kapp et al., 2005; Murphy et al., 1997). The inferred 55–64% shortening would then indeed require the removal of vast amounts of crust—equivalent to 20–40 km thickness (Fig. 2C–D) from the Pamir orogen by i) subhorizontal extrusion along strike, ii) erosion, or iii) return to the mantle (Fig. 6B). In this model, each of the Cenozoic Pamir domes was derived from the base of the pre-collisional normal-thickness crust or from middle or deeper levels of the crust thickened during the collision.

Substantial orogen-parallel extrusion in the Pamir is precluded by the prevalence of N–S stretching lineations at all exposed structural levels. Erosion certainly contributed to the removal of crust from the Pamir system, but is unlikely to have been the principal mechanism because i) low-grade sedimentary and volcanic sections are

Model A: 600 km shortening of thin crust; no excess crustal material



Model B: 900 km shortening of normal crust; 40 km thick layer of 'excess' crust

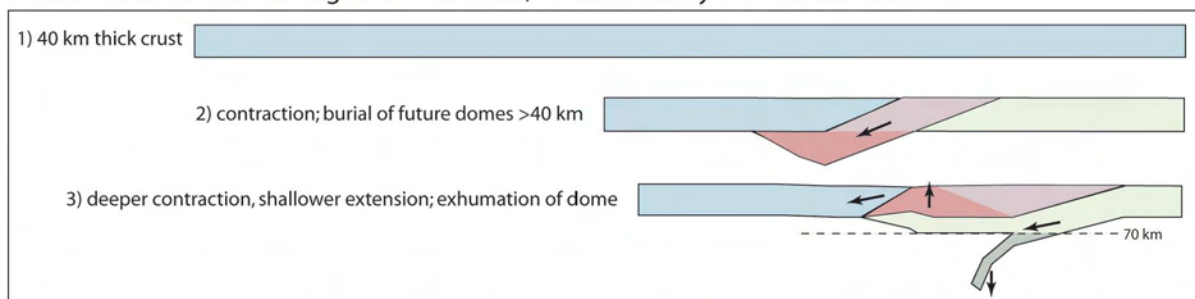


Fig. 6. The implications of the 30–40 km exhumation depths of the Cenozoic Pamir domes depend on the magnitude of shortening and the thickness of the pre-collisional crust. A) From a pre-collisional crustal thickness of 32 km, India–Asia convergence of 600 km can build a 70 km-thick crust with plane strain and no out-of-plane extrusion, erosion, or recycling of crust. Each dome (dark pink) represents a zone of unusually great exhumation and must be compensated by a corresponding zone of less exhumation. B) From a pre-collisional crustal thickness of 40 km, India–Asia convergence of 900 km builds a 70 km thick crust plus another 40 km of 'excess' crust that must be removed by out-of-plane extrusion, erosion, or recycling. Each dome was derived from the base of the pre-collisional normal-thickness crust or from middle or deeper levels of the crust thickened during the collision.

exposed across the Pamir (Vlasov et al., 1991); ii) zircon (U/Th)-He ages from the northern Pamir are Late Cretaceous to Eocene (Amidon and Hynek, 2010); and iii) the entire Tajik Depression contains only ~500,000 km³ of Cenozoic sediment (Brookfield and Hashmat, 2001), whereas just the northern half of the Pamir has a crustal volume ten times larger (400 km × 250 km × 70 km). Recycling of Pamir crust into the mantle is therefore likely to have occurred and is probably ongoing (Fig. 6B). This is documented by i) the late Miocene eruption of crustal xenoliths from 90–100 km depth in the southeastern Pamir (Hacker et al., 2005), and ii) earthquake hypocenters and seismic wavespeeds (Roecker, 1982).

6. Conclusions

Crystalline high-grade domes are exposed over a wide area of the Pamir. Thermobarometry yields peak P–T conditions for the domes of 6–14 kbar and 500–800 °C, corresponding to exhumation depths of 30–40 km. New titanite, zircon and monazite U/Th–Pb data plus existing geochronology indicate that most of the metamorphism—and, therefore, also the exhumation—occurred in the Oligo–Miocene. Both of these findings indicate that the Pamir are quite different than the Tibetan plateau, which has undergone minimal Cenozoic exhumation. The extensive and widespread exhumation of the deep Pamir crust is almost certainly a result of the India–Asia convergence being absorbed over a relatively narrow north–south distance. Whether the exhumation of the domes was accompanied by the subhorizontal extrusion, erosion, or folding of significant crustal mass hinges on the pre-collisional crustal thickness and the magnitude of shortening within the Pamir.

Acknowledgments

This material is based on work in the TIPAGE (Tien Shan–Pamir Geodynamic) initiative supported by the Deutsche Forschungsgemeinschaft (bundle 443 and Ra442/34) and the US National Science Foundation (EAR-0838269). The ion microprobe facility at UCLA is partly supported by a grant from the Instrumentation and Facilities Program, Division of Earth Sciences, National Science Foundation. Sample collection and interpretation of field relationships was completed during joint field work with M. Gadoev, R. Gloaguen, S. Gordon, J. Hofmann, E. Kanaev, I. Oimahmadov, D. Rutte, and K. Stanek. Alex Robinson and an anonymous reviewer contributed to the clarity and completeness of the presentation; Alex also generously shared a manuscript in review that helped crystalize our understanding of the northeastern Pamir.

Appendix A. Supplementary data

Supplementary data to this article can be found online at doi:10.1016/j.epsl.2011.10.034.

References

Aleinikoff, J.N., Wintsch, R.P., Fanning, C.M., Dorais, M.J., 2002. U–Pb geochronology of zircon and polygenetic titanite from the Glastonbury Complex, Connecticut, USA: an integrated SEM, EMPA, TIMS, and SHRIMP study. *Chem. Geol.* 188 (1–2), 125–147.

Amidon, W.H., Hynek, S.A., 2010. Exhumational history of the north central Pamir. *Tectonics* 29, TC5017. doi:10.1029/2009TC002589.

Bagdassarov, N., Batalev, V., Egorova, V., 2011. State of lithosphere beneath Tien Shan from petrology and electrical conductivity of xenoliths. *J. Geophys. Res.* 116. doi:10.1029/2009JB007125.

Brookfield, M.E., Hashmat, A., 2001. The geology and petroleum potential of the North Afghan Platform and adjacent areas (northern Afghanistan, with parts of southern Turkmenistan, Uzbekistan and Tajikistan). *Earth Sci. Rev.* 55 (1–2), 41–71.

Burtman, V.S., 2010. Tien Shan, Pamir, and Tibet: history and geodynamics of Phanerozoic oceanic basins. *Geotectonics* 44, 388–404.

Burtman, V.S., Molnar, P., 1993. Geological and geophysical evidence for deep subduction of continental crust beneath the Pamir. *Geol. Soc. Am. Spec. Pap.* 281, 1–76.

Cherniak, D.J., 1993. Lead diffusion in titanite and preliminary results on the effects of radiation damage on Pb transport. *Chem. Geol.* 110 (1–3), 177–194.

Cherniak, D.J., Pyle, J.M., 2008. Th diffusion in monazite. *Chem. Geol.* 256 (1–2), 52–61.

Connolly, J.A.D., 1990. Multivariable phase diagrams an algorithm based on generalized thermodynamics. *Am. J. Sci.* 290, 666–718.

DeCelles, P.G., Robinson, D.M., Zandt, G., 2002. Implications of shortening in the Himalayan fold–thrust belt for uplift of the Tibetan Plateau. *Tectonics* 21. doi:10.1029/2001TC001322.

DiPietro, J.A., Pogue, K.R., 2004. Tectonostratigraphic subdivisions of the Himalaya; a view from the west. *Tectonics* 23 (5), 20.

Doeblich, J.L., Wahl, R.R., 2006. Geologic and Mineral Resource Map of Afghanistan. US Geol. Surv.

Ducea, M.N., Lutkov, V., Minaev, V.T., Hacker, B., Ratschbacher, L., Luffi, P., Schwab, M., Gehrels, G.E., McWilliams, M., Vervoort, J., Metcalf, J., 2003. Building the Pamirs: the view from the underside. *Geology* 31, 849–852.

Ellis, D.J., Green, D.H., 1979. An experimental study of the effect of Ca upon garnet–clinopyroxene Fe–Mg exchange equilibria. *Contrib. Mineral. Petrol.* 71, 13–22.

Ferry, J.M., Spear, F.S., 1978. Experimental calibration of the partitioning of Fe and Mg between biotite and garnet. *Contrib. Mineral. Petrol.* 66, 113–117.

Frost, B.R., Chamberlain, K.R., Schumacher, J.C., 2000. Sphene (titanite): phase relations and role as a geochronometer. *Chem. Geol.* 172, 131–148.

Gerdes, A., Liu, F., Weyer, S., Brey, G., Anonymous, 2007. Chronological history of UHP rocks from the Chinese Continental Scientific Drilling; a multi-methodical approach. *Geochim. Cosmochim. Acta* 71 (15S), A317.

Ghent, E.D., 1976. Plagioclase–garnet–Al₂SiO₅–quartz: a potential geobarometer–geothermometer. *Am. Mineral.* 61, 710–714.

Ghent, E.D., Stout, M.Z., 1981. Geobarometry and geothermometry of plagioclase–biotite–garnet–muscovite assemblages. *Contrib. Mineral. Petrol.* 76, 92–97.

Gordon, S.M., Luffi, P.I., Hacker, B.R., Valley, J.W., Spicuzza, M., Kozdon, R., Kelemen, P., Ratschbacher, L., Minaev, V., in review. The thermal structure of continental crust in active orogens: Insight from Miocene eclogite- and granulite-facies xenoliths of the Pamir. *J. Metamorph. Geol.*

Graham, C.M., Powell, R., 1984. A garnet–hornblende geothermometer; calibration, testing, and application to the Pelona Schist, Southern California. *J. Metamorph. Geol.* 2, 13–31.

Grew, E.S., Pertsev, N.N., Yates, M.G., Christy, A.G., Marquez, N., Chernosky, J.C., 1994. Sapphirine + forsterite and sapphirine + humite-group minerals in an ultramagnesian lens from Kuhl-lal, SW Pamirs, Tajikistan: are these assemblages forbidden? *J. Petrol.* 35, 1275–1293.

Hacker, B.R., Luffi, P., Lutkov, V., Minaev, V., Ratschbacher, L., Plank, T., Ducea, M., Patiño-Douce, A., McWilliams, M., Metcalf, J., 2005. Near-ultrahigh pressure processing of continental crust: Miocene crustal xenoliths from the Pamir. *J. Petrol.* 46, 1661–1687.

Hacker, B.R., Wallis, S.R., Ratschbacher, L., Grove, M., Gehrels, G., 2006. High-temperature geochronology constraints on the tectonic history and architecture of the ultrahigh-pressure Dabie–Sulu orogen. *Tectonics* 25, TC5006. doi:10.1029/2001JB001129/2005TC001937.

Hacker, B.R., Kelemen, P.B., Behn, M.D., 2011. Differentiation of the continental crust by remelting. *Earth Planet. Sci. Lett.* 307, 501–516.

Hamburger, M.W., Sarewitz, D.R., Pavlis, T.L., Popandopopulo, G.A., 1992. Structural and seismic evidence for intracontinental subduction in the Peter the First Range, central Asia. *Geol. Soc. Am. Bull.* 104, 397–408.

Holland, T.J.B., Powell, R., 1998. An internally consistent thermodynamic data set for phases of petrological interest. *J. Metamorph. Geol.* 16, 309–343.

Hollister, L.S., 1966. Garnet zoning: an interpretation based on the Rayleigh fractionation model. *Science* 154, 1647–1651.

Hubbard, M.S., Grew, E.S., Hodges, K.V., Yates, M.G., Pertsev, N.N., 1999. Neogene cooling and exhumation of upper-amphibolite-facies ‘whiteschists’ in the southwest Pamir Mountains, Tajikistan. *Tectonophysics* 305, 325–337.

Jin, X., Wang, J., Chen, B., Ren, L., 2003. Cenozoic depositional sequences in the piedmont of the west Kunlun and their paleogeographic and tectonic implications. *J. Asian Earth Sci.* 21, 755–765.

Johnson, M.R.W., 2002. Shortening budgets and the role of continental subduction during the India–Asia collision. *Earth Sci. Rev.* 59, 101–123.

Kapp, P., Yin, A., Harrison, T.M., Ding, L., 2005. Cretaceous–Tertiary shortening, basin development, and volcanism in central Tibet. *Geol. Soc. Am. Bull.* 117, 865–878.

Kohn, M.J., Spear, F.S., 1990. Two new geobarometers for garnet amphibolites, with applications to southeastern Vermont. *Am. Mineral.* 75, 89–96.

Kohn, M.J., Spear, F., 2000. Retrograde net transfer reaction insurance for pressure–temperature estimates. *Geology* 28, 1127–1130.

Kretz, R., 1983. Symbols for rock-forming minerals. *Am. Mineral.* 68, 277–279.

Kylander-Clark, A.R.C., Hacker, B.R., Mattinson, J.M., 2008. Slow exhumation of UHP terranes: titanite and rutile ages of the Western Gneiss Region, Norway. *Earth Planet. Sci. Lett.* 272, 531–540.

Le Pichon, X., Fournier, M., Jolivet, L., 1992. Kinematics, topography, shortening, and extrusion in the India–Eurasia collision. *Tectonics* 11, 1085–1098.

Leonov, J.G., 1977. Materialien zur Geologie der Afgano-Tadschikischen Depression. *Academy of Sciences of U.S.S.R., problem commission 9, working group 3–3: “the tectonic regime of molasse-forming periods” report*, 50 pages (in Russian).

Ludwig, K.R., 2003. *Isoplot 3.00. A Geochronological Toolkit for Microsoft Excel*: Berkeley Geochronology Center Special Publication, 4.

McFarlane, C.R.M., Harrison, T.M., 2006. Pb-diffusion in monazite: constraints on a high-T contact aureole setting. *Earth Planet. Sci. Lett.* 250, 376–384.

Mechie, J., Kind, R., Saul, J., 2011. The seismological structure of the Tibetan Plateau crust and mantle down to 700 km depth. *Geol. Soc. Spec. Publ.* 353, 109–125.

Mechie, J., X. Yuan, X., Schurr, B., Schneider, F., Sippl, C., Ratschbacher, L., Minaev, V., Gadoev, M., Oimahmadov, I., Abdybachev, U., Moldobekov, B., Orunbaev, S., Negmatullayev, S., in review. Crustal structure along a profile across the Pamir and

- southern Tien Shan as derived from project TIPAGE wide-angle seismic data. *Geophys. J. Int.*
- Murphy, M.A., Yin, A., Garrison, T.M., Dürr, S.B., Chen, Z., 1997. Significant crustal shortening in south-central Tibet prior to the Indo-Asian collision. *Geology* 25, 719–722.
- Negredo, A., Replumaz, A., Villaseñor, A., Guillot, S., 2007. Modeling the evolution of continental subduction processes in the Pamir–Hindu Kush region. *Earth Planet. Sci. Lett.* 259, 212–225.
- Newton, R.C., Perkins, D.L., 1982. Thermodynamic calibration of geobarometers based on the assemblages garnet–plagioclase–orthopyroxene (clinopyroxene)–quartz. *Am. Mineral.* 67, 203–222.
- Pashkov, B.R., Dmitriyev, 1981. Muskol crystalline massif (central Pamir). *Int. Geol. Rev.* 24, 285–296.
- Peykre, Y.B., Pokhvisneva, Y.A., Zotov, I.A., 1981. The Muskol metamorphic complex of the Central Pamir. *Int. Geol. Rev.* 24, 297–303.
- Pidgeon, R.T., Bosch, D., Brugier, O., 1996. Inherited zircon and apatite U–Pb systems in an Archean syenite from southwestern Australia: implications for U–Pb stability of titanite. *Earth Planet. Sci. Lett.* 141, 187–198.
- Ratschbacher, L., Merle, O., Davy, P., Cobbold, P., 1991. Lateral extrusion in the eastern Alps, part 1: boundary conditions and experiments scaled for gravity. *Tectonics* 10, 245–256.
- Robinson, A.C., 2009. Geologic offsets across the northern Karakorum fault: implications for its role and terrane correlations in the western Himalayan–Tibetan orogen. *Earth Planet. Sci. Lett.* 279, 123–130.
- Robinson, A.C., Yin, A., Manning, C.E., Harrison, T.M., Zhang, S., Wang, X., 2004. Tectonic evolution of the northeastern Pamir; constraints from the northern portion of the Cenozoic Kongur Shan extensional system, western China. *Geol. Soc. Am. Bull.* 116, 953–973.
- Robinson, A.C., Yin, A., Manning, C.E., Harrison, T.M., Zhang, S.-H., Wang, X.-F., 2007. Cenozoic evolution of the eastern Pamir: implications for strain-accommodation mechanisms at the western end of the Himalayan–Tibetan orogen. *Geol. Soc. Am. Bull.* 119, 882–896.
- Robinson, A.C., Yin, A., Lovera, O., 2010. The role of footwall deformation and denudation in controlling cooling age patterns of detachment systems: an application to the Kongur Shan extensional system in the Eastern Pamir, China. *Tectonophysics* 496, 28–43.
- Roecker, S.W., 1982. Velocity structure of the Pamir–Hindu Kush region: possible evidence of subducted crust. *J. Geophys. Res.* 87, 945–959.
- Roger, F., Jolivet, M., Malavieille, J., 2008. Tectonic evolution of the Triassic fold belts of Tibet. *C.R. Geosci.* 340, 180–189.
- Schurr, B., Yuan, X., Mechie, J., Sippl, C., Schneider, F., Minaev, V., Abdybachev, U., 2009. A temporary seismological network across the Pamir and Tien Shan mountain ranges. *EOS Trans. Am. Geophys. Union* T43C–T2102C.
- Schwab, G., Katzung, G., Ludwig, A.O., Lützner, H., 1980. Neogene Molasse–Sedimentation in der Tadschikischen Depression (tadschikische SSR). *Z. Angew. Geol.* 26/5, 225–238.
- Schwab, M., Ratschbacher, L., Siebel, W., McWilliams, M., Lutkov, V., Minaev, V., Chen, F., Stanek, K., Nelson, B., Frisch, W., Wooden, J.L., 2004. Assembly of the Pamirs: age and origin of magmatic belts from the southern Tien Shan to the southern Pamirs and their relation to Tibet. *Tectonics* 23, TC4002. doi:10.1029/2003TC001583.
- Scott, D.J., St-Onge, M.R., 1995. Constraints on Pb closure temperature in titanite based on rocks from the Ungava Orogen, Canada; implications for U–Pb geochronology and P–T–t path determinations. *Geology (Boulder)* 23 (12), 1123–1126.
- Spencer, K., Hacker, B.R., Kylander–Clark, A.R.C., Cottle, J.M., Ginsburg, A., 2010. Determining the exhumation history of a giant UHP terrane using titanite geochronology, western gneiss region, Norway. *Geol. Soc. Am. Abstr. Programs* 42.
- Stübner, K., Ratschbacher, L., Weise, C., Pfänder, J., Gloguen, R., Hacker, B., Dunkl, I., Jonckheere, R., Stanek, K., Minaev, V., 2011. Miocene gneiss domes and syn-orogenic extension in the Pamir. Abstract EGU General Assembly, Vienna, Austria.
- Vielzeuf, D., Schmidt, M.W., 2001. Melting relations in hydrous systems revisited: application to metapelites, metagraywackes and metabasalts. *Contrib. Mineral. Petrol.* 141, 251–267.
- Vlasov, N.G., Y.A. Dyakov, and E.S. Cherev, Geological map of the Tajik SSR and adjacent territories, 1:500,000, Leningrad, 1991.
- Yardley, B.W.D., 1977. An empirical study of diffusion in garnet. *Am. Mineral.* 62, 793–800.